Paper submitted to MSM '99, San Juan, Puerto Rico, April 19-21, 1999

IMAP: Interferometry for Material Property Measurement in MEMS

Brian D. Jensen, Maarten P. de Boer, and Samuel L. Miller

Intelligent Micromachines Initiative, Dept. 1725
Sandia National Laboratories
Albuquerque, NM, USA
http://www.mdl.sandia.gov/Micromachine

ABSTRACT

An interferometric technique has been developed for non-destructive, high-confidence, *in-situ* determination of material properties in MEMS. By using interferometry to measure the full deflection curves of beams pulled toward the substrate under electrostatic loads, the actual behavior of the beams has been modeled. No other method for determining material properties allows such detailed knowledge of device behavior to be gathered. Values for material properties and non-idealities (such as support post compliance) have then been extracted which minimize the error between the measured and modeled deflections. High accuracy and resolution have been demonstrated, allowing the measurements to be used to enhance process control.

Keywords: optical measurement, material properties, interferometry

INTRODUCTION

Easy, high-confidence measurement of material properties is essential for optimizing micro-mechanical design and determining process control. Several methods have been suggested to determine simple properties such as Young's modulus and residual stress in the material. For example, Young's modulus has been measured using beam resonance [1], direct tensile testing [2, 3], and measurements of pull-in voltage [4, 5]. Residual stress measurements have been made from arrays of buckled beams [6], passive sensors which deform in a measurable way [7, 8], and measurements of pull-in voltage [4, 5].

Unfortunately, the accuracy of these methods varies greatly. Reported values for Young's modulus for polysilicon have ranged from 90 to 190 GPa [9]. Similarly, reported values for residual stress in polysilicon vary widely. While some variability is expected, the demonstrated accuracy and resolution of these techniques are not great enough to provide sufficient confidence in the data for valid process control. In addition, most of the methods cannot resolve values for residual stress below 1.0 MPa, even though good process control often requires keeping the stress near or below this level. Before a valid system of process control can be implemented, the demonstrated accuracy and resolution of measurement methods must be less than the expected variation due to the process. In addition, some non-idealities which commonly occur in micromachined structures cannot be detected or quantified using any of the previously suggested methods. Therefore, a need exists for high-confidence testing which provides the accuracy and resolution required for process control and design optimization.

Interferometry for material properties in MEMS (IMAP) is a high-resolution measurement technique which measures complete deflection curves of electrostatically-actuated micromachined beams to within approximately 10 nm, allowing these curves to be compared to modeled curves. Values for material properties are found which minimize the error between the modeled and measured deflection curves. This point-by-point comparison yields high confidence in the material properties, as well as the non-idealities, such as support post compliance, which are often ignored or not quantified using other techniques. In addition, the test is non-destructive, allowing prediction and verification of deflections at other loading conditions. By giving quick feedback to process engineers, as well as high confidence and reduced measurement variability, process control can be improved. The technique is illustrated using measurements made on beams fabricated using SUMMiT (Sandia Ultra-planar, Multi-level MEMS Technology), Sandia's polysilicon surface micromachining process [10].

METHOD

IMAP has been developed to allow extraction of strain gradient, Young's modulus, and film stress in four separate steps. First, the beam thickness and gap are measured using a profilometer. The deflection of an unloaded cantilever (fixed-free beam) is then measured optically, allowing extraction of the strain gradient. Young's modulus and the cantilever support post compliance are then found from the deflected shape of a loaded cantilever beam. Finally, the deflection curve of a fixed-fixed beam is used to find fixed-fixed beam support post compliance and residual stress.

Beam Thickness and Gap

Because the method relies on out-of plane deflections, the thickness and gap must be known precisely. The magnitude of the deflection depends on the thickness cubed and the gap squared, so that high-resolution measurement of these parameters is required. Most profilometry equipment can measure such dimensions quite well, though, with an accuracy of approximately 0.02 μm. For the beams measured here, the thickness is 2.32 μm, with a gap of 6.47 μm

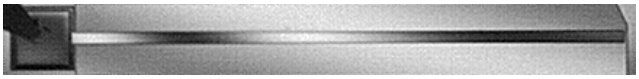

Figure 1: An interferogram of an unloaded 1,000 μm long cantilever

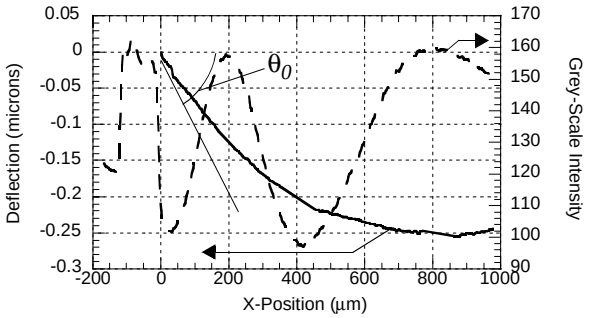

Figure 2: Grey-scale linescan and resulting deflection curve for the unloaded cantilever

Strain Gradient

The strain gradient through the thickness of a cantilever beam causes it to curve out of plane. Because this effect strongly influences the shape of a cantilever beam, it must be quantified before accurate measurement of Young's modulus may be made. It is also an important parameter for process control, as excessive curvature of the film may cause mechanical parts to mesh or interact incorrectly.

Residual strain gradient through the film thickness produces an internal moment, which causes the beam to deflect into a circular arc. Interferometry allows the deflected shape of the beam to be measured, from which the radius of curvature *R* of the circular arc may be found. For example, Figure 1 shows an interferometric image of a 1,000 μm cantilever beam. The fringes along the length of the beam indicate its out-of-plane deflection. The experimental setup is explained in [16]. By analyzing a grey-scale linescan, the complete deflection curve of the beam may be generated, as shown in Figure 2.

Some imperfections in the interferometry data had to be considered and accounted for. For example, although the background fringes in Figure 1 are not parallel with the beam's length, this has been corrected in the deflection curve by using a linear correction factor. In addition, the deflections extremely close to the support posts are difficult to measure because the optical data becomes mixed with data from the support pad. Also, for images with few fringes, the data is more noisy near maxima and minima of the linescan. These effects concern only a small portion of the total curve, though, so that they can usually be ignored.

The deflection curve in Figure 2 may be described as an arc with radius of curvature of 1.1×10^{6} μm, with an initial angle of $\theta_0 = 6.2\times10^{-4}$ radians. Both of these parameters are vital pieces of information necessary for subsequent modeling. However, they have generally been ignored or inferred, rather than directly measured, by other material property measurement methods. The detailed data derived from interferometry allows direct measurement of such non-idealities, which are then incorporated into the modeling. The initial angle θ_0 of the unloaded cantilever is probably due to process issues as well as the complex interactions occurring between film stress and strain gradient at the support post [11, 12].

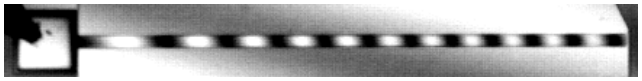

Figure 3: The interferogram of a 1,000 μm long loaded cantilever at 3.8 V

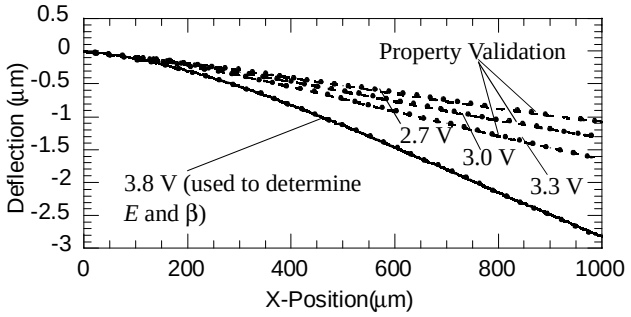

Figure 4: A graph showing the measured and modeled deflections for various loads on the cantilever beam

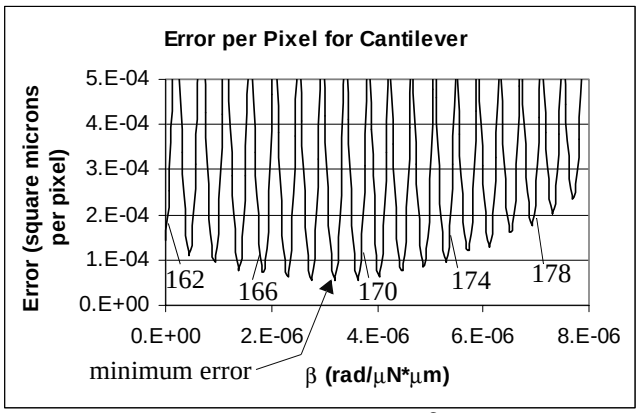

Figure 5: Error as a function of *E* and β for the 1,000 μm cantilever. Different values for *E* are labeled in GPa.

Young's Modulus

With the beam thickness, gap, initial angle, and strain gradient known, Young's modulus is measured using the deflected shape of a cantilever beam pulled toward the substrate by electrostatic forces. This is done by finding the value which minimizes the error between a model of the beam's deflection and the deflected beam shape. Cantilever support post compliance is measured simultaneously.

Figure 3 shows the 1,000 μm beam deflected under an applied voltage of 3.8 V. The linescan and analysis produces the measured deflection curve shown for the 3.8 V-curve in Figure 4. The modeled curve which lies over the measured data points in the figure was produced by performing a search for the best fit over a range of Young's modulus, *E*, and support post compliance, β. Figure 5 shows the results of this search, indicating that the best value for *E* lies between

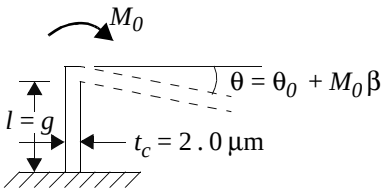

Figure 6: The beam support post model

168 and 170 GPa. This graph is generated by interpolating into the modeled deflection at each measured point (corresponding to one pixel). The error at each point is squared, summed over all points, and divided by the total number of points. The absolute minimum is found at E = 169 GPa, with β equal to 3.2×10^{-6} rad/μN-μm.

The model used to arrive at these results consists of an automated routine which divides the beam into a number of beam elements. It then iteratively applies the fringing-field-corrected electrostatic load to each element, calculates internal forces and moments, and finds the resulting deflection shape based on Young's modulus, support post compliance, unloaded support post angle, and strain gradient. The cycle continues until convergence is reached.

The support post is modeled simply as a cantilever beam subjected to an end moment, as shown in Figure 6 [13]. The total initial angle θ of the deflected beam is found as the sum of the unloaded support post angle, found previously using Figure 2, and the angle induced due to bending of the support post. This induced angle is equal to the product of the end moment M_0 and the parameter β [14]. An equivalent thickness t_c of the support post may also be extracted [13].

If the width of the beam is large compared to its thickness, then the plate modulus D, which depends on E and Poisson's ratio, must be used in place of E [14]. Osterberg and Senturia recommend using D in place of E if the width is more than five times the thickness [5]. For the beams presented here, D was used, with Poisson's ratio assumed to be 0.23.

To check the result found for the 1,000 μm beam, the deflection of a 600 μm beam was also measured and compared to the model. For this beam, the minimum error was found for E between 170 and 173 GPa and β between 2.4 and 3.5×10^{-6} rad/μN-μm. Therefore, the best value for E is chosen to be 170±3 GPa. Using E = 170 GPa and $\beta = 3.5\times10^{-6}$ rad/μN-μm, which corresponds to t_c = 2.0 μm, deflections for the 1,000 μm beam were predicted at 3.3, 3,0, and 2.7 V. The results are presented in Figure 4. The good agreement between predicted and measured deflections provides high confidence in the measured value of E.

Residual Stress

As fixed-fixed beams deflect, the axial force through the beam causes stiffening to occur, changing the deflection of the beam. Because residual stress is an important part of this axial force, the deflected shape of the beam depends strongly on the magnitude of the residual stress. Either tensile or compressive residual stresses may be measured.

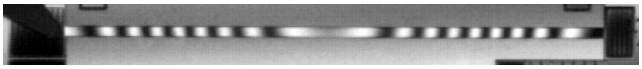

Figure 7: A 1,000 μm fixed-fixed beam under 25.1 V

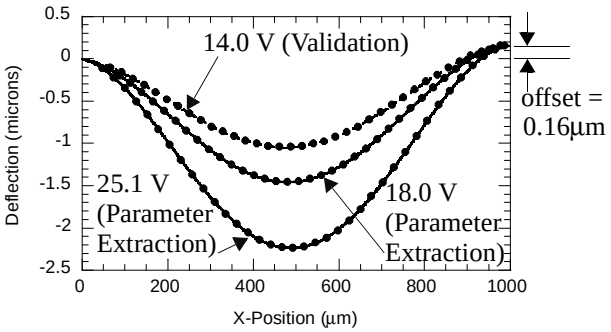

Figure 8: Measured (dots) and modeled (lines) deflections of a fixed-fixed beam

Figure 7 shows a 1,000 μm fixed-fixed beam deflected under a potential of 25.1 V. The deflection curve of the beam, the lowest curve in Figure 8, indicates that the right support post is about 0.16 μm higher than the other. The difference in height between the two support posts was independently verified using SEM images. Such a large difference would not be expected from conventional surface micromachining processes; however, it can result from global non-uniformities introduced in an oxide surface after a CMP step. Research is underway to reduce the global non-uniformity, and process and design methods have been suggested to help control it [15]. Interferometry allows this height offset to be directly measured.

Because the interferometry data conclusively shows that the support posts are at different heights, the model was extended to account for the asymmetry. Also, in the iterative beam deflection solution, support post compliance is introduced by allowing the two ends of the beam to take on any given end angle θ within a reasonable range. This simplifies the mathematics in the iterative solution, improving convergence. Therefore, in finding the best value for residual stress, the optimal slope at each end of the beam must also be found.

To determine the true residual stress in the beam the axial deflection Δ at the support posts must also be found. Because this deflection is small, typically on the order of 1 nm, modeling must be used in place of measurement. The support posts are again modeled as short cantilever beams like the one in Figure 6. An addition required to the model is the presence of the fixed-fixed beam's axial force as an end load. However, the support posts for the fixed-fixed beam have a different design, so that the cantilever support post compliance cannot be assumed. Instead, it can be measured by comparing the deflections of the beam at two values of voltage. Then, the best value of residual stress can be found for each deflection measurement. These extracted values of residual stress are not expected to be the same because they do not include the effect of Δ. However, by comparing the

Table 1: Δ and True Residual Stress

Voltage	Δ_{left}, μm	Δ_{right}, μm	σ_R (true), MPa
18.0V	-1.6×10^{-4}	-3.9×10^{-4}	-3.00
25.1V	2.7×10^{-4}	7.9×10^{-4}	-3.01

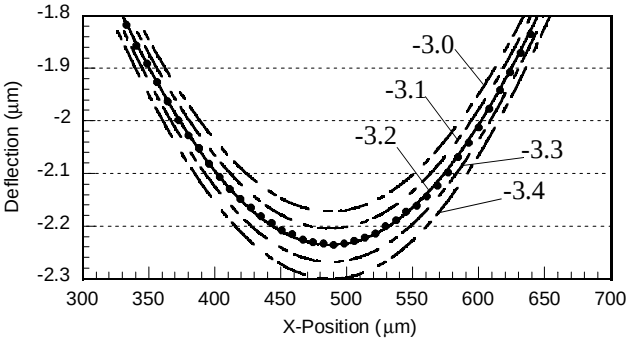

Figure 9: Modeled deflections (lines) at several stress levels (in MPa) compared to the measured deflection (dots) as an indication of measurement resolution

axial force and the end slopes and moments for each deflection curve, values for Δ at each post may be found, leading to a calculation of true residual stress.

For the 1,000 μm beam, deflections were measured and modeled for two deflections, at 18.0 V and 25.1 V. To find the best value for residual stress, a search was made over a range of values for residual stress, left post slope, and right post slope. As expected, the extracted values of residual stress, which were not compensated for differences in Δ, were not identical. The best fit occurred for -3.2 MPa for the 25.1 V deflection and -2.9 MPa for the 18.0 V deflection. The negative stress value indicates compression. By comparing the two, Δ and true residual stress are extracted. The values are shown in Table 1. To further test the measurement, the deflection of the beam under 14 V potential was measured and modeled, as shown in Figure 8. The resulting best-fit, uncompensated residual stress was -2.7 MPa. The corrected residual stress was -2.8 MPa, within 0.2 MPa of the measured value.

To study the resolution of the method, the deflection curves at a series of stress levels were modeled and compared to the measured deflection at 25.1 V. The result is shown in Figure 9. A difference of 0.1 MPa causes a change in maximum deflection of about 20 to 40 nm, which is well resolved using the interferometry. Therefore, we have gained high confidence in the measured stress value of -2.9±0.1 MPa, and we can now use this value to improve process control, especially to help ensure that future films are deposited in tension, which is the desired state.

CONCLUSION

IMAP is a method to accurately determine material properties in MEMS. Interferometry has allowed the development of accurate models for beam deflections, leading to high confidence in both the boundary conditions and mechanical property values. Our measurements showed E = 170±3 GPa and σ_R = -2.9±0.1 MPa for polysilicon beams. Further, the interferometric measurements have led to a better understanding of the process, illustrated by the unloaded beam angles and the disparate heights of the fixed-fixed beam pads. The continuation of this work will enable accurate feedback for both process engineers and designers. Future work includes studying a variety of boundary designs to find an optimized design, as well as correlating support post models with FEM.

ACKNOWLEDGMENTS

The assistance of Daniel Gutierrez in gathering the interferometry data is gratefully acknowledged. Technical discussions and data from Jeff Sniegowski are also appreciated, as is the fabrication work of the staff of Sandia's Microelectronics Development Laboratory. Sandia is a multiprogram laboratory operated by Sandia Corporation, a Lockheed Martin Company, for the United States Department of Energy under Contract DE-AC04-94AL85000.

REFERENCES

[1] Kiesewetter, L, Zhang, J-M, Houdeau, D, and Steckenborn, A, *Sensors and Actuators A*, **35**, 1992, 153-159.
[2] Sharpe, W, Yuan, B, Vaidyanathan, R, and Edwards, R, *SPIE 1996*, **2880**, 78-91.
[3] Chasiotis, I and Knauss, W, *SPIE 1998*, **3512**, 66-75.
[4] Gupta, R, Osterberg, P, and Senturia, S, *SPIE 1996*, **2880**, 39-45.
[5] Osterberg, P and Senturia, D, *J. MEMS*, **6**(2), 1997, 107-118.
[6] Guckel, H, Burns, D, Rutigliano, C, Lovell, E, and Choi, B, *J. Micromech. Microeng.*, **2**, 1992, 86-95.
[7] Gianchandani, Y and Najafi, K, *J. MEMS*, **5**(1), 1996, 52-58.
[8] Ericson, F, Greek, S, Söderkvist, J, and Schweitz, J-Å, *J. Micromech. Microeng.*, **7**, 1997, 30-36.
[9] Schweitz, J-Å, *MRS Bulletin*, July 1992, 34-45.
[10] http://www.mdl.sandia.gov/Micromachine
[11] Lober, T, Huang, S, Schmidt, M, and Senturia, S, *Hilton Head 1988*, 92-95.
[12] Fang, W and Wickert, J, *J. Micromech. Microeng.*, **5**, 1995, 276-281.
[13] Meng, Q, Mehregany, M. and Mullen, Robert, *J. MEMS*, **2**(3), 1993, 128-137.
[14] Timoshenko, S and Woinowsky-Krieger, S, *Theory of Plates and Shells*, McGraw-Hill, 4-32, 1959.
[15] Hetherington, D, and Sniegowski, J, *SPIE 1998*, San Diego, Ca, July 1998.
[16] de Boer, M, Tabbara, M, Dugger, M, Clews, P, and Michalske, T, *Transducers '97*, 229-232.